Journal of Thermal Engineering
Web page info: https://jten.yildiz.edu.tr
DOI: 10.14744/thermal.0000957

Research Article

Effects of radiation and chemical reaction due to graphene oxide nanofluid flow in concentric cylinders

Jagadeeshwar PASHIKANTI[1,*], Susmitha PRIYADHARSHINI D R[1], Santhosh THOTA[1]

[1]*Department of Science and Humanities, Indian Institute of Information Technology Tiruchirappalli Tamil Nadu 620012, India*

ARTICLE INFO

Article history
Received: 7 January 2024
Revised: 12 July 2024
Accepted: 04 August 2024

Keywords:
Buongiorno Model; Entropy Generation; Graphene Nanofluids

ABSTRACT

Aggregated studies on thermal radiation effects in nanofluid flow are important for the effective utilization of its striking thermophysical properties and extensive industrial applications such as coolants in automobile radiators, heat exchangers, propulsion systems, atomic plants, etc. Particularly in concentric cylinders, the nanofluid flow has a wide range of applications, including medicine such as stenosis treatment. This investigation is one such computational study to explore the radiative flow between two concentric cylinders due to graphene oxide nanofluids. The flow is modeled, including the impacts of radiative heat flux, chemical reaction effects, thermophoresis, and Brownian motion. The spectral method is used to solve the system of complex nonlinear coupled equations under convective conditions. The influence of implanted parameters on skin friction, concentration, and temperature profiles of the nanofluid and their impacts on entropy are studied. From the tabulated values of the Sherwood and Nusselt numbers, it is observed that convective heat and mass transfer can be enhanced by the thermophoresis parameter and the Brownian motion parameter, whereas diffusive mass transfer is enhanced by the chemical reaction parameter. A comparison table shows good agreement between the literature and the obtained values. Also, the results obtained are graphed and discussed in detail, along with entropy generation.

Cite this article as: Pashikanti J, Priyadharshini D R S, Thota S. Effects of radiation and chemical reaction due to graphene oxide nanofluid flow in concentric cylinders. J Ther Eng 2025;11(4):970–981.

INTRODUCTION

Nanofluids are used to overcome the drawbacks of microfluids and viscous fluids, such as the erosion of flow channels, clogging, and deposition. While modeling their flow, thermophoretic diffusion and Brownian motion are considered for their significance in heat and mass transfer [1]. Besides the advantages of nanofluids on the whole, the type of nanoparticles dispersed in the fluids greatly influence the behavior of the nanofluids. In view of their thermophysical properties, graphene nanoparticles are the best choice for enhanced thermal performance. They significantly improve the performance of fluids in devices such as radiators and heat exchangers when dispersed either as nanoparticles or hybrid nanoparticles [2, 3, 4, 5].

*Corresponding author.
*E-mail address: jagadeeshwarp@iiitt.ac.in, jagadeeshwar.pashikanti@gmail.com

This paper was recommended for publication in revised form by Editor-in-Chief Ahmet Selim Dalkılıç

Published by Yıldız Technical University Press, İstanbul, Turkey

The commonly used graphene nanofluids in literature are graphene oxide nanofluids and composite graphene nanofluids with ethylene glycol and water as basefluids [1]. Azimi et al.[6] evaluated the heat transfer analytically when graphene oxide nanofluid flows unsteadily within moving plates. In their study, a comparative analysis is conducted by dispersing GO, alumina, titania, and silver nanoparticles and it is interpreted that silver nanofluid was effected in the highest Nusselt number and it increased with volume fraction. Gul et al. [7] examined the 2D flow in an upright channel. In this study, the authors concluded that GO with ethylene glycol has stronger thermal efficiency than water-based GO. While Ullah et al. [8] examined the 3D flow where the fluid is pressed between a vertical channel. Both investigations emphasize the impacts of strong magnetic effects on nanofluid flow when the medium is considered to be porous and concluded that magnetic field parameter controlled the fluid flow. The slip flow of titanium dioxide and graphene oxide nanofluids using the Levenberg-Marquardt scheme in neural networks is studied by Khan et al. [9]. The influence of flow variables on velocity, temperature, and concentration profiles are discussed and the absolute error values are found to range between 10^{-1} to 10^{-8}.

Extensive applications of thermal radiation and chemical reaction effects in different propulsion systems, atomic plants, turbines, the manufacturing of polymers, fertilizers, and dyes, etc. signify their importance in Computational Fluid Dynamics. Noteworthy investigations considering the impacts of chemical reaction and thermal radiation, such as the study by Srinivasacharya and Ayano [10], investigated the impacts of chemical reaction on a micropolar fluid with MHD and cross-diffusion effects, with the conclusion that the microrotation, velocity, and concentration profiles decayed with chemical reaction parameter. Srinivasacharya and Shafeeurrahman [11] investigated the flow of a chemically reacting nanofluid for entropy generation analysis with magnetic field and Joule heating effect. From the results obtained, it is concluded that the entropy, velocity, and temperature of the nanofluid are enhanced by the Joule heating parameter, whereas, the velocity is enhanced and the temperature and entropy generation are depleted by the chemical reaction parameter. Masood and Farooq [12] conducted an analysis on thermal stratification and thermal radiation effects due to the MHD flow of graphene oxide and silver nanoparticles in water. The inferences of this investigation are that convective heat transfer decreases with both the stratification parameter and radiation parameter. Jha and Samaila [13] studied the impacts of thermal radiation and nonlinear density variation on the MHD flow over an inclined plate. The results show an elevation in heat transfer with angle of inclination and thermal radiation. Oyedepo et al. [14] modeled the thermal performance of alumina nanofluids as coolants in car radiators. Results signified a 14% elevation in heat transfer coefficient for a 4% increase in volume fraction. Rathore and Sandeep [15] modelled and investigated the blood-based silver and gold nanofluid flow in a stenosed artery with variable heat source and magnetic field effects. This study helps with localized photothermal therapy (PTT) to treat cancer. Algehyne et al. [16] computationally examined the hybrid nanofluid flow due to partially ionized graphene oxide and silver over a stretching sheet. The investigation signifies a decrease in velocity with Hartmann number and an increase with Hall current and ion-slip parameter.

Moreover, many classical and novel methods for numerical and analytical investigations in cylindrical geometries have been widely used. For example, Zeeshan et al. topologically approached the flow of nanofluids using a combined Genetic algorithm and Nelder-Mead method [17] with the conclusion that the Dufour number and the Dufour-solutal Lewis number enhance the Sherwood number while depleting the Nusselt number. Kumar et al. [18] explored the study on Powell-Eyring fluid flow in concentric rotating cylinders and found from the results obtained that the velocity profiles increase with the Powell-Eyring parameter and rotation parameter. [19] investigated fractional Oldroyd-B nanofluid for 1-D flow with ethylene glycol-based molybdenum disulfide, copper, alumina, and silver nanoparticles. The conclusions suggest that molybdenum disulfide nanofluid has higher velocity profiles in comparison to the other nanofluids. Studies such as the analysis of the squeezing flow of an ionic liquid by Shah et al. [20] with a conclusion that copper nanoparticles among copper, alumina, and titania are the best to enhance heat transfer is worth mentioning. Also, an enhancement in the velocity boundary layer is found to be unique to copper nanofluids. A numerical examination of nanofluid flow in a porous annulus is conducted by Miles and Bessaih [21] and entropy and convective heat transfer are observed to increase with the addition of nanoparticles.

Limited applied and computational studies on graphene nanofluids demand further exploration of their flow. Also, thermal radiation and chemical reaction effects have extensive industrial applications, such as the manufacturing of dyes, fertilizers, and polymers, spacecraft, turbines, atomic plants, missiles, satellites, etc. Despite all the computational investigations on concentric cylinders, there is a lack of literature on the convective study due to graphene oxide nanofluid flow with chemical reaction effects and thermal radiation impacts in concentric cylinders. The investigation aims to bridge the gap by studying the flow of graphene oxide nanoparticles in water between concentric cylinders. The modeled equations are numerically solved, and the values are graphically represented.

GOVERNING EQUATIONS

The geometry of the flow consists of an inner vertical cylinder placed concentrically with an outer cylinder of radii a and b, respectively. The following assumptions are made to model the flow between the vertical cylinders.

- Graphene oxide nanofluid is assumed to flow with constant pressure gradient $\partial P/\partial \Theta$.

- The flow is driven by the rotation of the outer cylinder which has an angular velocity Ω.
- u is the tangential velocity with which the fluid flows.
- The flow is steady, incompressible, axisymmetric, and fully developed meaning the fluid has constant density, the equations describing the flow are the same at any point throughout the channel and are independent of time, and angular coordinate.
- The body forces due to gravity, radiative heat flux, and chemical reaction effects, the effects caused by characteristic nanoparticle phenomena namely thermophoresis and Brownian motion are considered.

The outline of the flow model is shown in Figure 1. Implementing the above-mentioned assumptions, Boussinesq approximations, and boundary layer approximations, the variations with respect to axial coordinate disappear. Thus the governing partial differential equations of the problem adapting Buongiorno nanofluid model [22] are given by,

$$\frac{\partial u}{\partial \Theta} = 0 \tag{1}$$

$$\frac{\rho_{nf} u^2}{r} = \frac{\partial p}{\partial r} \tag{2}$$

$$\mu_{nf}\left(\frac{\partial^2 u}{\partial r^2} + \frac{1}{r}\frac{\partial u}{\partial r} - \frac{u}{r^2}\right) + (1 - C_a)(T - T_a)g(\rho\beta)_{nf} - (\rho_p - \rho_{bf})(C - C_a)g - \frac{1}{r}\frac{\partial p}{\partial \Theta} = 0 \tag{3}$$

$$\frac{\kappa_{nf}}{(\rho C_p)_{nf}}\left(\frac{\partial^2 T}{\partial r^2} + \frac{1}{r}\frac{\partial T}{\partial r}\right) + \tau\left(D_{DB}\left(\frac{\partial T}{\partial r}\frac{\partial C}{\partial r}\right) + \frac{D_T}{T_a}\left(\frac{\partial T}{\partial r}\right)^2\right) - \frac{1}{(\rho C_p)_{nf} r}\frac{\partial (r q_r)}{\partial r} = 0 \tag{4}$$

$$D_B\left(\frac{\partial^2 C}{\partial r^2} + \frac{1}{r}\frac{\partial C}{\partial r}\right) + \frac{D_T}{T_a}\left(\frac{\partial^2 T}{\partial r^2} + \frac{1}{r}\frac{\partial T}{\partial r}\right) - K_C(C - C_a) = 0 \tag{5}$$

along with the following no-slip convective boundary conditions [23]

$$u = 0,\ -\kappa_{nf}\frac{\partial T}{\partial r} = h(T_a - T), -D_m\frac{\partial C}{\partial r} = k_m(C_a - C),\ \text{at } r = a$$

$$u = b\Omega,\ -\kappa_{nf}\frac{\partial T}{\partial r} = h(T - T_b), -D_m\frac{\partial C}{\partial r} = k_m(C - C_b),\ \text{at } r = b \tag{6}$$

Here, the equations (1) - (5) respectively represent the nanofluid continuity equation, r–momentum equation, Θ–momentum equation, energy equation, nanoparticle continuity equation [24]. The notations T_b, T_a, C_b, and C_a indicate the fluid temperature and concentration at the outer and inner cylinders respectively, k_m and h are mass and heat transfer coefficients, and Dm denotes mass diffusivity and κ thermal conductivity.

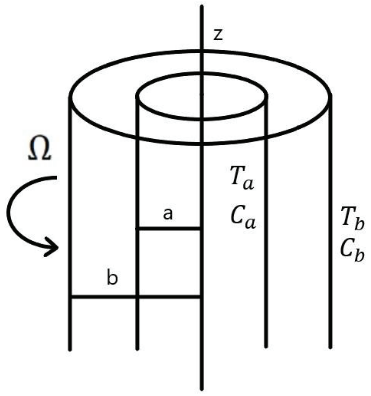

Figure 1. Outline of the flow in concentric cylinders (created by the author).

Let σ^* be Stefan's constant and k^* be Roseland's mean absorption coefficient, then radiative heat flux is represented by $q_r = (-4\sigma^*/3k^*)(\partial T^4/\partial r)$. T^4 is expanded in Taylor series about T_a to obtain $T^4_a \approxeq 4T^3_a\, T - 3T^4_a$ by ignoring the higher order derivatives.

Properties of nanofluids are defined as [7, 29]

Table 1. Thermophysical properties [25, 26, 27, 28]

Property (Units)	Water	GO
$\rho\,(kg/m^3)$	997.1	1800
$C_p\,(J/kg\,K)$	4179	717
$\kappa\,(W/mK)$	0.613	5000
$\beta\,(10^{-5}/K)$	21	28.4

$$\mu_{nf} = \frac{\mu_{bf}}{(1-\Phi)^{2.5}},\ \alpha_{nf} = \frac{\kappa_{nf}}{(\rho C_p)_{nf}},$$

$$\rho_{nf} = (1-\Phi)\rho_{bf} + \Phi\rho_{sp},$$

$$(\rho\beta)_{nf} = (1-\Phi)(\rho\beta)_{bf} + \Phi(\rho\beta)_{sp}$$

$$(\rho C_p)_{nf} = (1-\Phi)(\rho C_p)_{bf} + \Phi(\rho C_p)_{sp},$$

$$\frac{\kappa_{nf}}{\kappa_{bf}} = \frac{\kappa_{sp} + 2\kappa_{bf} + 2\Phi(\kappa_{bf} - \kappa_{sp})}{\kappa_{sp} + 2\kappa_{bf} - \Phi(\kappa_{bf} - \kappa_{sp})}$$

The suffixes *bf, sp* and *nf* refer to base fluid, nanofluid, and solid particle and the quantities defined above are respectively viscosity, thermal diffusivity, density, thermal expansion coefficient, specific heat capacity, and thermal conductivity. Table 1 presents the values of thermophysical properties.

The idea of similarity transformation broadly refers to the transformation of the given problem to a similar and simpler problem using the variables called similarity variables. In this study, it displays the physical similarities within the given problem such as the similarities of velocity, temperature, and concentration profiles.

These variables are used to reduce the number of independent variables of the problem under consideration. The transformation of the partial differential equations is achieved through the similarity variables,

$$\eta = \frac{r^2}{b^2},\ u = \frac{\Omega}{\sqrt{\eta}} f(\eta),\ \theta(\eta) = \frac{T - T_a}{T_f - T_a},$$
$$\phi(\eta) = \frac{C - C_a}{C_f - C_a},\ P = \frac{pb}{\Omega \mu_{bf}} \quad (7)$$

Thus, the equations (1) - (6) are transformed as:

$$4\eta f'' + A_1 \frac{Gr}{Re}\sqrt{\eta}(A_2\theta - Nr\phi) - A_1 P_1 = 0 \quad (8)$$

$$(1 + A_3 R_d)(\eta\theta'' + \theta') + A_4 \eta\theta'(N_b\phi' + N_t\theta') = 0 \quad (9)$$

$$\eta\phi'' + \phi' + \frac{N_t}{N_b}(\eta\theta'' + \theta') + \frac{C_R Sc}{4}\phi = 0 \quad (10)$$

Similarly, the boundary conditions are

$$\text{at } \eta = \eta_0 = \frac{a^2}{b^2},\ f = 0,\ 2\sqrt{\eta_0}\theta' = A_3 Bi_t \theta,$$
$$2\sqrt{\eta_0}\phi' = Bi_c(1 - \phi)$$
$$\text{at } \eta = 1,\ f = 1,\ 2\theta' = A_3 Bi_t(1 - \theta),$$
$$2\phi' = Bi_c(1 - \phi) \quad (11)$$

The constants A_i, $i = 1$ to 4 and the coefficients in the above equations namely the Grashof number G_r, Reynolds number Re, buoyancy ratio N_r, radiation parameter R_d, Brownian motion parameter N_b, chemical reaction parameter C_R, thermophoresis parameter N_t, constant pressure gradient P_1, Schmidt number Sc, thermal diffusivity α_{nf}, thermal and concentration Biot number Bi_t and Bi_c and heat capacity ratio τ are defined as

$$A_1 = (1 - \Phi)^{2.5},\ A_2 = 1 - \Phi + \Phi\frac{(\rho\beta)_{sp}}{(\rho\beta)_{bf}},\ A_3 = \frac{\kappa_{bf}}{\kappa_{nf}},$$
$$A_4 = 1 - \Phi + \Phi\frac{(\rho C_p)_{sp}}{(\rho C_p)_{bf}}\frac{\kappa_{bf}}{\kappa_{nf}},$$

$$Gr = \frac{\rho_{bf}^2 g\beta(T_b - T_a)(1 - C_a)b^3}{\mu_{bf}^2},\ Re = \frac{\rho_{bf}\Omega b}{\mu_{bf}},$$
$$N_r = \frac{(\rho_{sp} - \rho_{bf})(C_b - C_a)}{(\rho\beta)_{bf}(1 - C_a)(T_b - T_a)},$$

$$N_b = \frac{\tau D_B(C_b - C_a)}{\alpha_{nf}},\ N_t = \frac{\tau D_T(T_b - T_a)}{T_a\alpha_{nf}},$$
$$R_d = \frac{-16\sigma^*}{k^*\kappa_{bf}}T_a^3,\ C_R = \frac{-\rho_{bf}K_C b^2}{\mu_{bf}},$$

$$Bi_t = \frac{hb}{\kappa_{bf}},\ Bi_c = \frac{k_m b}{D_m},\ \tau = \frac{(\rho C_p)_{sp}}{(\rho C_p)_{nf}},$$
$$P_1 = \frac{1}{\mu_{bf}\Omega}\frac{\partial P}{\partial\Theta},\ \alpha_{nf} = \frac{\kappa_{bf}}{(\rho C_p)_{bf}},\ Sc = \frac{\mu_{bf}}{\rho_{bf}D_B}.$$

The derived practically important quantities such as local Sherwood number Sh_z and Nusselt number Nu_z and skin friction C_f are

$$\frac{Nu_\eta}{2} = -(1 + A_4 R_d)\theta'(1),\ \frac{Sh_\eta}{2} = -\phi'(1),$$
$$\eta C_f Re_\eta = A_5(f'(1) - f(1)) \quad (12)$$

where $A_5 = 4(1 - \Phi)^{-2.5}((1-\Phi)+\Phi\rho^{sp}/\rho_{bf})^{-1}$. The entropy generation number is derived and assessed in the next section.

Analysis on Entropy Generation

The entropy generation rate, [30]

$$S_G = \frac{\kappa_{nf}}{T_a^2}\left(1 + \frac{16\sigma^*}{k^*\kappa_{nf}}\right)\left(\frac{\partial T}{\partial r}\right)^2 + \frac{\mu_{nf}}{T_a}\left(\frac{\partial u}{\partial r} - \frac{u}{r}\right)^2$$
$$+ RD_B\left(\frac{\partial C}{\partial r}\right)\left(\frac{1}{C_a}\left(\frac{\partial C}{\partial r}\right) + \frac{1}{T_a}\left(\frac{\partial T}{\partial r}\right)\right), \quad (13)$$

is composed of entropy due to temperature, viscous dissipation, and concentration. From the characteristic entropy generation rate $S_{G0} = \kappa_{nf}(T_b - T_a)^2/(T_a L)^2$ and S_G, entropy generation number can be written as

$$N_S = \frac{S_G}{S_{G_0}} \quad (14)$$

On nondimensionalization,

$$\frac{\eta^2}{4}N_S = \frac{1}{\chi}\left((1 + A_4 R_d)\eta^3\theta'^2 + A_7\frac{EcPr}{\Omega_T}(\eta f' - f)^2\right.$$
$$\left. + A_4 M_m\frac{\Omega_C}{\Omega_T}\phi'\left(\frac{\Omega_C}{\Omega_T}\phi' + \theta'\right)\right) \quad (15)$$

$$= N_{S_h} + N_{S_f} + N_{S_m}, \quad (16)$$

where the total entropy number is composed of three parts, the entropy number due to combined mass and heat transfer N_{Sm}, fluid friction N_{Sf} and heat transfer N_{Sh}. The nondimensional parameters in (15) are defined as Eckert number $Ec = \Omega^2/(C_{pbf}(T_b - T_a))$, Prandtl number $Pr = \mu_{bf}C_{pbf}/\kappa_{bf}$, constant parameter $\chi = d^2/L^2$, temperature parameter

$\Omega_T = (T_b - T_a)/T_a$, concentration parameter $\Omega_C = (C_b - C_a)/C_a$ and the combined mass and heat transfer parameter $M_m = RD_BC_a/\kappa_{bf}$.

By estimating Bejan number $Be = N_{Sh}/N_S$ [31], the cause for generated entropy is determined. Bejan number, if > 0.5, heat transfer is influenced, if < 0.5, combined heat and mass transfer and fluid friction is the major cause, and if = 0.5, all the three irreversibilities contribute equally [32].

NUMERICAL SOLUTION

The Spectral quasilinearization method (SQLM) [23, 33, 34] is used to solve the equations (8) - (11). This technique has been successfully used in a limited number of studies and is shown to give better accuracy at lower orders than the spectral homotopy analysis method converges rapidly, and is thus superior to some semi-analytical methods such as the Adomian decomposition method, the Laplace transform decomposition technique, the variational iteration method, and the homotopy perturbation method. The SLM and SQLM are non-perturbation methods requiring neither the presence of an embedded perturbation parameter nor the addition of an artificial parameter. These methods are therefore free of the major limitations associated with other perturbation methods. Nonlinear terms are linearised by ignoring the higher derivatives in Taylor series expansion about the solution. Let f_r, θ_r and ϕ_r and f_{r+1}, θ_{r+1} and ϕ_{r+1} be the solutions and improved solutions of the differential equations. Thus, the linearised equations with the boundary conditions are

$$a_{1,r}f_{r+1}'' + a_{2,r}\theta_{r+1} + a_{3,r}\phi_{r+1} = p_r \tag{17}$$

$$b_{1,r}\theta_{r+1}'' + b_{2,r}\theta_{r+1}' + b_{3,r}\phi_{r+1}' = q_r \tag{18}$$

$$c_{1,r}\theta_{r+1}'' + c_{2,r}\theta_{r+1}' + c_{3,r}\phi_{r+1}'' + c_{4,r}\phi_{r+1} = 0 \tag{19}$$

such that

$$\begin{aligned} &\text{at } \eta = \eta_0,\ f_{r+1} = 0,\ 2\sqrt{\eta_0}\theta_{r+1}' = \theta_{r+1}A_3Bi_t, \\ &2\sqrt{\eta_0}\phi_{r+1}' = Bi_c(1 - \phi_{r+1}) \\ &\text{at } \eta = 1,\ f_{r+1} = 1,\ 2\theta_{r+1}' = A_3Bi_t(1 - \theta_{r+1}), \\ &2\phi_{r+1}' = Bi_c(1 - \phi_{r+1}) \end{aligned} \tag{20}$$

The coefficients are given by

$$a_{1,r} = 4\eta,\ a_{2,r} = A_1A_2\frac{Gr}{Re}\sqrt{\eta},$$
$$a_{3,r} = -A_1N_r\frac{Gr}{Re}\sqrt{\eta},$$

$$b_{1,r} = (1 + A_3R_d)\eta,\ b_{2,r} = 1 + A_3R_d + A_4\eta(N_b\phi_r' + 2N_t\theta_r')$$
$$b_{3,r} = A_4N_b\eta\theta_r',$$

$$c_{1,r} = \frac{N_t}{N_b}\eta,\ c_{2,r} = \frac{N_t}{N_b},\ c_{3,r} = \eta,\ c_{4,r} = C_RSc,$$
$$p_r = A_1P_1,\ q_r = A_4\eta(N_b\theta_r'\phi_r' + N_t\theta_r'^2)$$

Chebyshev polynomials $T_k(\xi) = cos(k\ cos^{-1}(\xi))$ are used and f, θ and ϕ are iterated at $\xi_j = cos\ (\pi j/N)$, $j = 0, 1, 2, \ldots N$, the Gauss Lobatto collocation points and the domain $[\eta_0, 1]$ is mapped to these points by $\eta = \{(1-\eta_0)\xi+(1+\eta_0)\}/2$. Thus, the unknowns and their derivatives are given by

$$\begin{aligned} f_{r+1}(\xi) &\cong \textstyle\sum_{k=0}^{N} f_{r+1}(\xi_k)T_k(\xi_j), \\ \theta_{r+1}(\xi) &\cong \textstyle\sum_{k=0}^{N} \theta_{r+1}(\xi_k)T_k(\xi_j), \\ \phi_{r+1}(\xi) &\cong \textstyle\sum_{k=0}^{N} \phi_{r+1}(\xi_k)T_k(\xi_j) \end{aligned} \tag{21}$$

$$\begin{aligned} \frac{d^r f_{r+1}}{d\eta^r} &= \textstyle\sum_{k=0}^{N} D_{kj}^r\, f_{r+1}(\xi_k), \\ \frac{d^r \theta_{r+1}}{d\eta^r} &= \textstyle\sum_{k=0}^{N} D_{kj}^r\, \theta_{r+1}(\xi_k), \\ \frac{d^r \phi_{r+1}}{d\eta^r} &= \textstyle\sum_{k=0}^{N} D_{kj}^r\, \phi_{r+1}(\xi_k) \end{aligned} \tag{22}$$

Here, the Chebyshev differentiation matrix is given by $D = D/2$. Substitution of the above approximations in (17) - (20) yields,

$$\mathcal{A}\mathcal{Y}_{r+1} = \mathcal{R}_r \tag{23}$$

associated with the boundary conditions

$$\begin{aligned} &f_{r+1}(\xi_0) = b, \\ &\&(2D_{00} + A_3Bi_t)\theta_{r+1}(\xi_0) \\ &+2\textstyle\sum_{k=1}^{N} D_{0k}\,\theta_{r+1}(\xi_k) = A_3Bi_t(2D_{00} + Bi_c)\phi_{r+1}(\xi_0) \\ &+2\textstyle\sum_{k=1}^{N} D_{0k}\,\phi_{r+1}(\xi_k) = Bi_c \end{aligned} \tag{24}$$

$$f_{r+1}(\xi_N) = 0,\ 2\sqrt{\eta_0}\sum_{k=0}^{N-1} D_{Nk}\,\theta_{r+1}(\xi_k)$$
$$+(2\sqrt{\eta_0}D_{NN} - A_3Bi_t)\theta_{r+1}(\xi_N) = 0$$

$$2\sqrt{\eta_0}\sum_{k=0}^{N-1} D_{Nk}\,\phi_{r+1}(\xi_k) + (2\sqrt{\eta_0}D_{NN} - Bi_c)\phi_{r+1}(\xi_N) = 0$$

We choose the initial functions as $f_0 = (\eta-\eta_0)/(1-\eta_0)$, $\theta_0 = \{A_3Bi_t(\eta-\eta_0)+2\sqrt{\eta_0}\}/\ \{A_3Bi_t(1-\eta_0)+2(1+\sqrt{\eta_0})\}$, $\phi_0 = \{Bi_c(\eta-\eta_0)+2\sqrt{\eta_0}\}\ /\ \{Bi_c(1-\eta_0)+2(1+\sqrt{\eta_0})\}$ to satisfy the boundary conditions (20). These initial conditions are iterated to obtain the numerical solution.

RESULTS AND DISCUSSION

The numerical results of temperature, velocity, and concentration are estimated in the section for varied values in the practical range [35, 36]. Parameter values are taken as $Bi_t = 0.8$, $Bi_c = 0.3$, $Gr = 2 \times 10^5$, $N_b = 2\times10^{-4}$, $Re = 300$, $N_t = 3\times10^{-4}$, $Nr = 2$, $Sc = 170$, $R^d = 5$ and $C_R = 0.08$ unless mentioned otherwise and $Pr = 6.5$ and $\Phi = 0.01$. SLM approximation of 100th order is taken to obtain converging results at the third iteration. The results for the case of $Gr = P_1 = R_d$

$= C_R = 0$, from the present study are compared to the results from Sinha and Chaudhary [37] in Table 3 and the values are observed to be in good agreement.

Figures 2 - 4 depict the influence of *Re* on *f*, N_S and *Be*. As the Reynolds number increases, viscous forces increase and hence the flow velocity is supposed to increase. But in this case, the velocity is observed to decrease due to the presence of thermal radiation (Fig. 2). Similarly, the entropy number also decreases (Fig. 3) increasing the Bejan number and suggesting that the entropy comes from mass transfer and fluid friction (Fig. 4).

Figures 5 - 8 represent the effects of Bi_t on f, θ, N_S and *Be*. When Bit increases, velocity slightly decreases (Fig. 5). Whereas, increasing the Bi_t improves the heat transfer coefficient thus increasing the heat transfer from the inner to outer cylinder. Hence, there is a rise in the temperature of the nanofluid at the outer cylinder, whereas the temperature falls at the inner cylinder (Fig. 6). From Fig. 7, it is observed that N_S increases with the values of Bi_t. This is because the increasing heat transfer coefficient improves the nanofluid temperature.

An increase in temperature means that the particles of the substance have greater kinetic energy. The faster-moving particles have more disorder than particles that are moving slowly at a lower temperature, and hence N_S increases. This results in an increased *Be*, thus emphasizing the dominance of heat transfer on the increased entropy (Fig. 8).

The impacts of Bic on f, ϕ, N_S, and *Be* are shown in Figures 9 - 12. An increase in Bi_c boosts the mass transfer by enhancing the coefficient of convective mass transfer. This results in an enhanced nanofluid velocity (Fig. 9). The enhanced mass transfer aids in the movement of nanoparticles from the inner to outer cylinder, thus causing increased concentration values at the outer cylinder and decreased values at the inner cylinder (Fig. 10). Whereas, N_S increases for $\eta < 0.386$, again increases for $0.386 < \eta <$

Table 2. Nusselt number, Sherwood number, and skin friction values

Re	N_b	N_t	Bi_t	Bi_c	R_d	C_R	$-\theta'(1)$	$-\phi'(1)$	$A_5(f'(1) - f(1))$
100	0.0003	0.0002	0.8	0.3	5	0.08	-0.493155	-0.141261	-882.895175
300	0.0003	0.0002	0.8	0.3	5	0.08	-0.493155	-0.141261	-293.824076
500	0.0003	0.0002	0.8	0.3	5	0.08	-0.493155	-0.141261	-176.009856
700	0.0003	0.0002	0.8	0.3	5	0.08	-0.493155	-0.141261	-125.518048
300	0.0001	0.0002	0.8	0.3	5	0.08	-0.493156	-0.141261	-293.823815
300	0.0002	0.0002	0.8	0.3	5	0.08	-0.493156	-0.141261	-293.823956
300	0.0003	0.0002	0.8	0.3	5	0.08	-0.493155	-0.141261	-293.824076
300	0.0004	0.0002	0.8	0.3	5	0.08	-0.493154	-0.141261	-293.824191
300	0.0003	0.0002	0.8	0.3	5	0.08	-0.493155	-0.141261	-293.824076
300	0.0003	0.0003	0.8	0.3	5	0.08	-0.493154	-0.141261	-293.824252
300	0.0003	0.0004	0.8	0.3	5	0.08	-0.493153	-0.141261	-293.824417
300	0.0003	0.0005	0.8	0.3	5	0.08	-0.493152	-0.141261	-293.824572
300	0.0003	0.0002	0.1	0.3	5	0.08	-0.073806	-0.141261	-292.972292
300	0.0003	0.0002	0.3	0.3	5	0.08	-0.209604	-0.141261	-293.248136
300	0.0003	0.0002	0.5	0.3	5	0.08	-0.331643	-0.141261	-293.496024
300	0.0003	0.0002	0.7	0.3	5	0.08	-0.441913	-0.141261	-293.719999
300	0.0003	0.0002	0.8	0.2	5	0.08	-0.493156	-0.096018	-296.534858
300	0.0003	0.0002	0.8	0.4	5	0.08	-0.493154	-0.184837	-291.308222
300	0.0003	0.0002	0.8	0.6	5	0.08	-0.493153	-0.267437	-286.79676
300	0.0003	0.0002	0.8	0.8	5	0.08	-0.493152	-0.344609	-282.887564
300	0.0003	0.0002	0.8	0.3	1	0.08	-0.162747	-0.141261	-293.82552
300	0.0003	0.0002	0.8	0.3	2	0.08	-0.245349	-0.141261	-293.824795
300	0.0003	0.0002	0.8	0.3	3	0.08	-0.327951	-0.141261	-293.824434
300	0.0003	0.0002	0.8	0.3	4	0.08	-0.410553	-0.141261	-293.824219
300	0.0003	0.0002	0.8	0.3	5	0.01	-0.493155	-0.141764	-296.560056
300	0.0003	0.0002	0.8	0.3	5	0.015	-0.493155	-0.141572	-295.514781
300	0.0003	0.0002	0.8	0.3	5	0.02	-0.493155	-0.141476	-294.99353
300	0.0003	0.0002	0.8	0.3	5	0.025	-0.493155	-0.141419	-294.681221

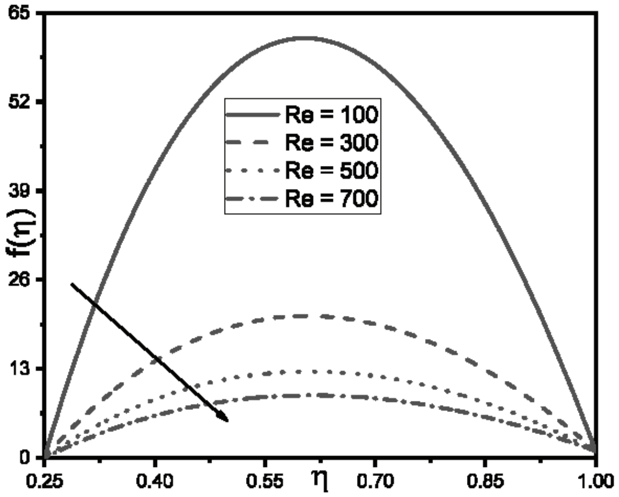

Figure 2. Influence of *Re* on *f*.

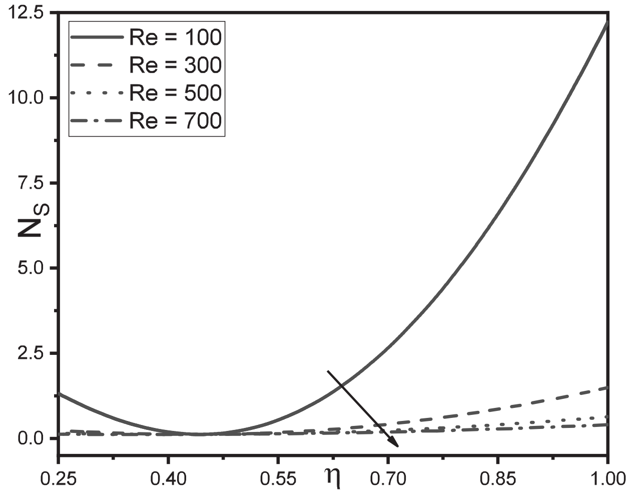

Figure 3. Influence of *Re* on N_S.

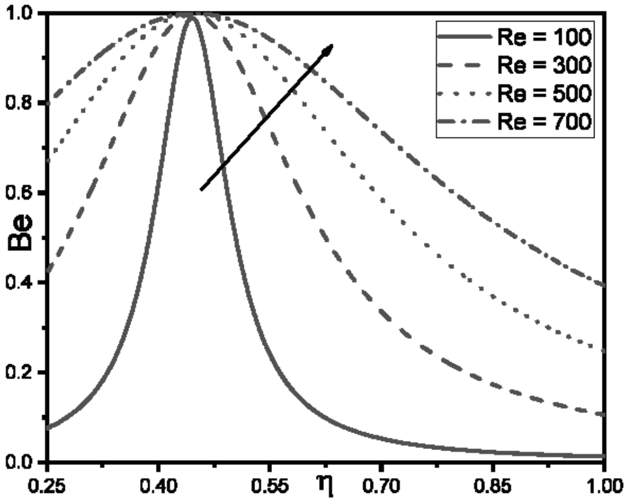

Figure 4. Influence of *Re* on *Be.*

0.906 and decreases for $\eta > 0.906$ (Fig. 11). This results in a decreasing *Be* for $\eta < 0.386$, decreasing for $0.386 < \eta < 0.906$ and increasing for $\eta > 0.906$ (Fig. 12). Hence, fluid friction and mass transfer influence the entropy all over the flow channel.

The effects of R_d *and* C_R *on* N_S and *Be* and ϕ are respectively presented in Figures 13 - 15. When the radiation parameter is increased, N_S increases (Fig. 13). But the impact of R_d on the temperature profile is ineffective. Thus, from this, we infer that the heat transfer effected by radiative heat flux completely vanishes in the generated entropy. Considering the Bejan number, increasing N_S causes *Be* to increase (Fig. 14), thus affirming the influence of heat transfer on the increasing entropy when the radiation parameter is involved. Likewise, when the values of C_R are raised, the enhancing rate of chemical reaction propagates the nanoparticle concentration. Hence, when C_R is increased, there is an inflation ϕ values (Fig. 15).

Table 2 shows *Nu, Sh* and *Cf* values at the outer cylindrical surface. Nusselt number is the ratio between convection to conduction at the surface, and at the surface, *Nu* increases with increasing Bi_c. This implies that the convection at the outer surface increases with diffusion and convective mass transfer, because, as the concentration Biot number is increased, convective mass transfer improves and the nanoparticles move with higher kinetic energy, thus improving the surficial heat transfer by convection. Whereas, Nu decreases with Bit and Rd, thus enhancing the conductive heat transfer. The impact of R_d on *Nu* also explains its ineffectiveness on the temperature profile. Whereas the impact of Bi_t on *Nu* emphasizes that the increased θ profiles were due to conduction and

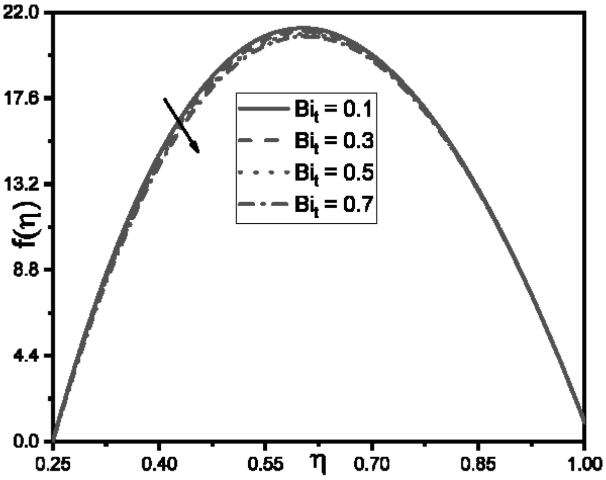

Figure 5. Influence of Bi_t on f

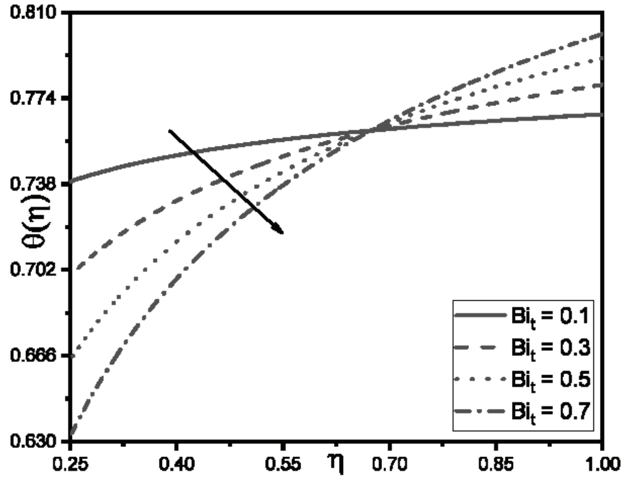

Figure 6. Influence of Bi_t on θ.

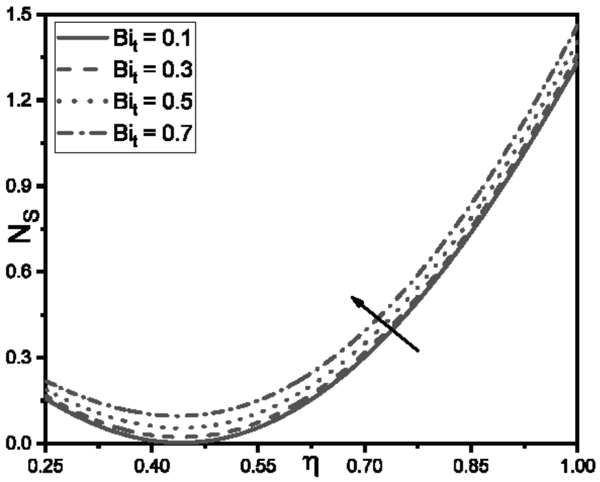

Figure 7. Influence of Bi_t on N_S.

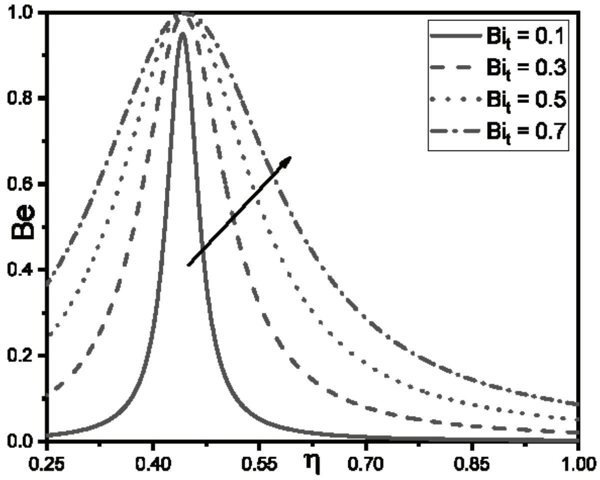

Figure 8. Influence of Bi_t on Be.

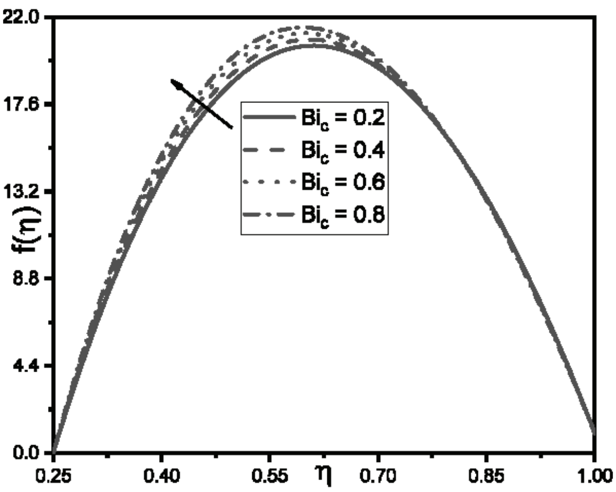

Figure 9. Influence of Bi_c on f.

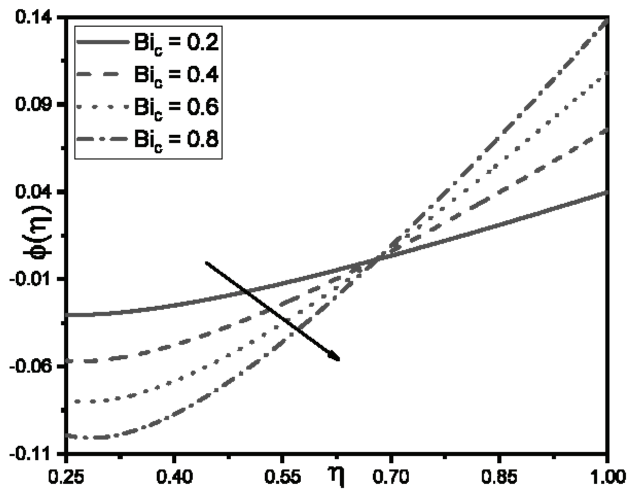

Figure 10. Influence of Bi_c on ϕ.

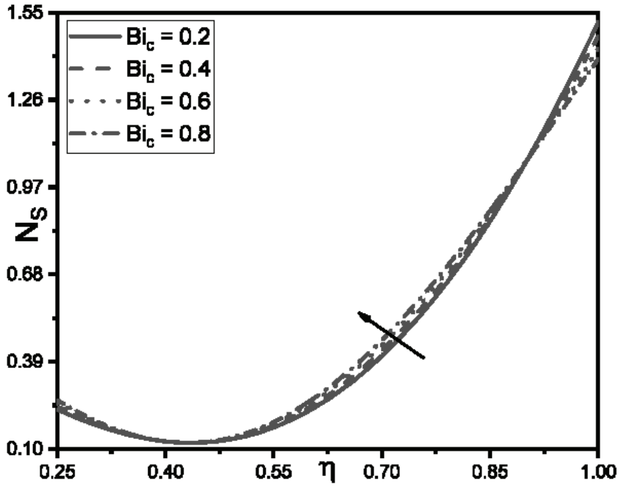

Figure 11. Influence of Bi_c on N_S.

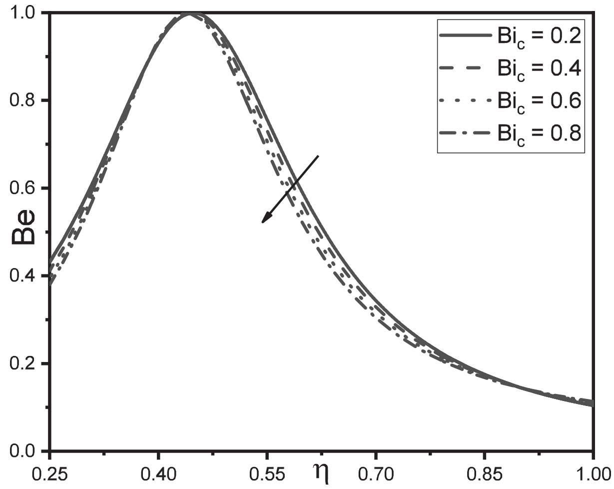

Figure 12. Influence of Bi_c on Be.

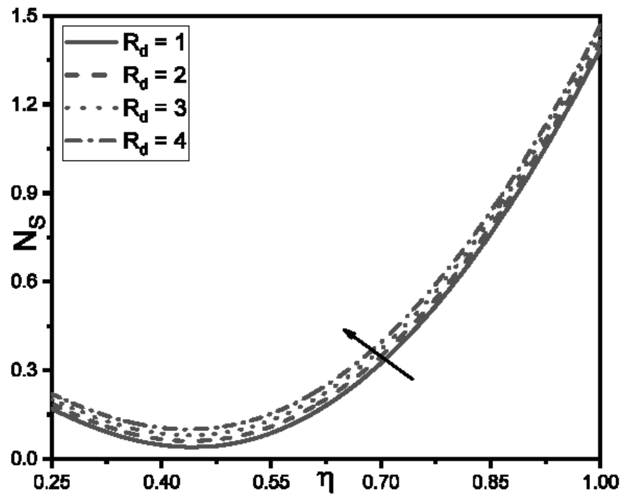

Figure 13. Influence of R_d on N_S.

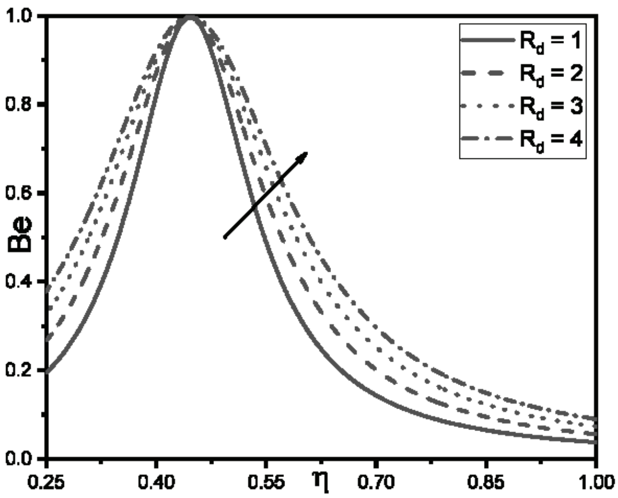

Figure 14. Influence of R_d on Be.

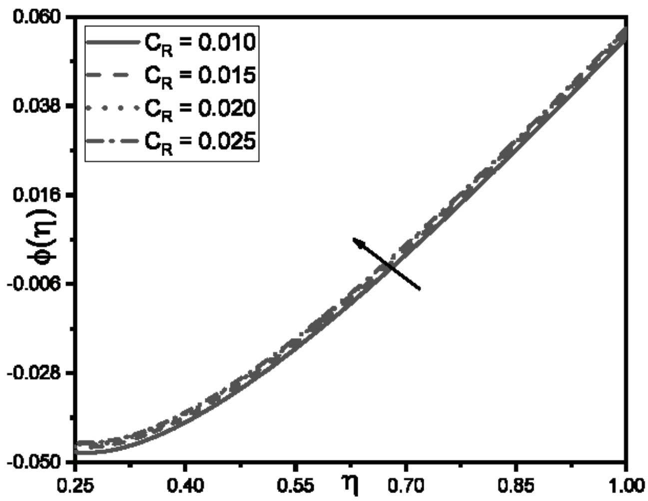

Figure 15. Influence of R_d on ϕ.

Table 3. $f(\eta)$ values for $Gr = P_1 = R_d = C_R = 0$

η	Present study	Sinha and Chaudhary [37]
1	1	1
0.98165	0.97553	0.97546
0.92838	0.90451	0.90453
0.84542	0.79389	0.79386
0.74088	0.65451	0.65453
0.625	0.5	0.5
0.50912	0.34549	0.34546
0.40458	0.20611	0.20613
0.32162	0.095492	0.09546
0.26835	0.024472	0.02453
0.25	0	0

not convection, as expected. Similarly, when Bi_c and C_R increase, the values of Sh decreases and increases respectively. Thus, the concentration Biot number enhances the concentration profiles in view of diffusion and not convection, similar to the case of Bi_t. While C_R enhances the rate of chemical reaction consequently enhancing convective mass transfer at the surface. Similarly, the skin friction drag, even if it is very small is impacted by the embedded parameters. Moreover, Bi_t reduces the skin friction by enhancing the nanoparticle characteristics, while Re, Bi_c, R_d and C_R elevate the skin friction drag at the surface.

CONCLUSION

Flow of graphene oxide nanofluid between concentric cylinders with the effects of thermal radiation and chemical reaction parameter is studied and the following are inferred:

- Heat transfer is enhanced by thermal Biot number.
- Mass transfer is increased by chemical reaction parameter and concentration Biot number.
- Skin friction is preferably reduced by enhancing the thermophoresis parameter, Brownian motion parameter, and thermal Biot number.
- Bejan number is calculated to be Be > 0.5 for η > 0.625, and hence the generated entropy is due to heat transfer close to the outer cylinder.
- Enhancing the radiation parameter depletes the Nusselt number and increases skin friction and enhancing the chemical reaction parameter enhances the Sherwood number and skin friction.

The problem is useful widely ranging from turbine manufacturing, aircraft propulsion systems, coolants, automobile radiators, and heat exchangers to pharmacotherapy. The study can be extended by analyzing the non-Newtonian behavior of the fluid.

NOMENCLATURE

Bi_c	concentration Biot number
Bi_t	thermal Biot number
C	concentration of the nanofluid
C_a	concentration of the nanofluid at the inner cylinder
C_b	concentration of the nanofluid at the outer cylinder
C_f	skin friction
C_p	specific heat capacity $(JK^{-1}kg^{-1})$
C_R	chemical reaction parameter
D_B	Brownian diffusivity (m^2s^{-1})
D_T	thermophoretic diffusivity (m^2s^{-1})
Ec	Eckert number
f	dimensionless velocity
g	acceleration due to gravity (ms^{-2})
Gr	Grashof number
h	heat transfer coefficient $(Wm^{-2}K^{-1})$
k	mass transfer coefficient (ms^{-1})
K_C	rate of chemical reaction (s^{-1})
M_m	heat parameter
N_b	Brownian diffusion coefficient number
Nr	buoyancy ratio
N_S	dimensionless entropy generation number
N_t	thermophoretic diffusion coefficient number
N_{Sm}	entropy due to combined heat and mass transfer
Nu	Nusselt number
P	dimensionless pressure
p	pressure (Pa)
Pr	Prandtl number
q_r	radiative heat flux (Wm^{-2})
R	universal gas constant
r	radial co-ordinate
R_d	radiation parameter
Re	Reynolds number
S_G	entropy generation rate
Sc	Schmidt number
Sh	Sherwood number
T	Nanofluid temperature (K)
T_a	Nanofluid temperature at the inner cylinder (K)
T_b	Nanofluid temperature at the outer cylinder (K)
u	tangential velocity component (ms^{-1})

Greek symbols

α_{nf}	thermal diffusivity (m^2s^{-1})
β	thermal expansion coefficient (K^{-1})
χ	constant parameter
η	similarity variable
κ	thermal conductivity $(Wm^{-1}K^{-1})$
λ	mixed convection parameter
μ	dynamic viscosity (Nsm−2)
Ω	angular velocity (rad s−1)
Ω_C	concentration parameter
Ω_T	temperature parameter
Φ	nanoparticle volume fraction
ϕ	dimensionless concentration
ψ	stream function

ρ density *(kgm^{-3})*
τ heat capacity ratio
Θ tangential coordinate
θ dimensionless temperature
θ_r variable viscosity parameter

Subscripts
bf base fluid
nf nanofluid
sp solid particle

ACKNOWLEDGEMENT

This research received no specific grant from any funding agency in the public, commercial, or not-for-profit sectors.

AUTHORSHIP CONTRIBUTIONS

Authors equally contributed to this work.

DATA AVAILABILITY STATEMENT

The authors confirm that the data that supports the findings of this study are available within the article. Raw data that support the finding of this study are available from the corresponding author, upon reasonable request.

CONFLICT OF INTEREST

The author declared no potential conflicts of interest with respect to the research, authorship, and/or publication of this article.

ETHICS

There are no ethical issues with the publication of this manuscript.

STATEMENT ON THE USE OF ARTIFICIAL INTELLIGENCE

Artificial intelligence was not used in the preparation of the article.

REFERENCES

[1] Barai DP, Bhanvase BA, Sonawane SH. A review on graphene derivatives-based nanofluids: Investigation on properties and heat transfer characteristics. Ind Eng Chem Res 2020;59:10231−10277. [CrossRef]
[2] Kumar R, Verma SK. Exergetic and energetic evaluation of an innovative solar air heating system coated with graphene and copper oxide nano-particles. J Therm Eng 2021;7:447−467. [CrossRef]
[3] Madderla S, Ramasamy D, Sudhakar K, Kadirgama K, Harun WSW. Heat transfer performance of a radiator with and without louvered strip by using graphene-based nanofluids. J Therm Eng 2021;7:1315−1328. [CrossRef]
[4] Barai R, Kumar D, Wankhade A. Heat transfer performance of nanofluids in heat exchanger: A review. J Therm Eng 2023;9:86−106. [CrossRef]
[5] Pandey H, Gupta NK, Agarwal S. An experimental investigation to study the performance characteristics of heat pipe using aqueous hybrid nanofluids. J Therm Eng 2021;9:1130−1139. [CrossRef]
[6] Azimi M, Azimi A, Mirzaei M. Investigation of the unsteady graphene oxide nanofluid flow between two moving plates. J Comput Theor Nanosci 2014;11:2104−2108. [CrossRef]
[7] Gul T, Ullah MZ, Alzahrani AK, Amiri IS. Thermal performance of the graphene oxide nanofluids flow in an upright channel through a permeable medium. IEEE Access 2019;7:102345−102355. [CrossRef]
[8] Ullah MZ, Gul T, Alshomrani AS, Baleanu D. The natural convective graphene oxide nanofluid-flow in an upright squeezing channel. Therm Sci 2019;23:S1981−S1989. [CrossRef]
[9] Khan MI, Shoaib M, Zubair G, Kumar RN, Prasannakumara BC, Mousa AAA, et al. Neural artificial networking for nonlinear Darcy−Forchheimer nanofluidic slip flow. Appl Nanosci 2023;13:3767−3786. [CrossRef]
[10] Srinivasacharya D, Shiferaw M. Cross diffusion effects on chemically reacting magnetohydrodynamic micropolar fluid between concentric cylinders. J Heat Transf 2013;135:122003. [CrossRef]
[11] Srinivasacharya D, Shafeeurrahman M. Joule heating effect on entropy generation in MHD mixed convection flow of chemically reacting nanofluid between two concentric cylinders. Int J Heat Technol 2017;35:487−497. [CrossRef]
[12] Masood S, Farooq M. Influence of thermal stratification and thermal radiation on graphene oxide-Ag/H_2O hybrid nanofluid. J Therm Anal Calorim 2021;143:1361−1370. [CrossRef]
[13] Jha BK, Samaila G. Nonlinear approximation for buoyancy-driven mixed convection heat and mass transfer flow over an inclined porous plate with Joule heating, nonlinear thermal radiation, viscous dissipation, and thermophoresis effects. Numer Heat Transf B Fundam 2023;83:139−161. [CrossRef]
[14] Oyedepo SO, Ezeuduji D, Araoyinbo AO, Kilanko O, Efemwenkiekie UK, Dirisu JO, et al. Numerical modeling of heat transfer performance and optimization of car radiator using (H_2O/Al_2O_3) nanofluids as coolant. Numer Heat Transf B Fundam 2022;82:185−198. [CrossRef]
[15] Rathore N, Sandeep N. Computational framework on heat diffusion in blood-based hybrid nanoliquid flow through a stenosed artery: An aligned magnetic field application. Numer Heat Transf B Fundam 2023;83:162−175. [CrossRef]

[16] Algehyne EA, Alharbi AF, Saeed A, Dawar A, Ramzan M, Kumam P. Analysis of the MHD partially ionized GO-Ag/water and GO-Ag/kerosene oil hybrid nanofluids flow over a stretching surface with Cattaneo–Christov double diffusion model: A comparative study. Int Commun Heat Mass Transf 2022;136:106205. [CrossRef]
[17] Zeeshan A, Baig M, Ellahi R, Hayat T. Flow of viscous nanofluid between the concentric cylinders. J Comput Theor Nanosci 2014;11:646–654. [CrossRef]
[18] Kumar D, Ramesh K, Chandok S. Mathematical modeling and simulation for the flow of magneto-Powell-Eyring fluid in an annulus with concentric rotating cylinders. Chin J Phys 2020;65:187–197. [CrossRef]
[19] Abro KA, Abdon A. A computational technique for thermal analysis in coaxial cylinder of one-dimensional flow of fractional Oldroyd-B nanofluid. Int J Ambient Energy 2022;43:5357–5365. [CrossRef]
[20] Shah RA, Ullah H, Khan MS, Khan A. Parametric analysis of the heat transfer behavior of the nano-particle ionic-liquid flow between concentric cylinders. Adv Mech Eng 2021;13:16878140211024009. [CrossRef]
[21] Miles A, Bessaïh R. Heat transfer and entropy generation analysis of three-dimensional nanofluids flow in a cylindrical annulus filled with porous media. Int Commun Heat Mass Transf 2021;124:105240. [CrossRef]
[22] Buongiorno J. Convective transport in nanofluids. J Heat Transf 2006;128:240–250. [CrossRef]
[23] Srinivasacharya D, Bindu KH. Entropy generation in a micropolar fluid flow through an inclined channel with slip and convective boundary conditions. Energy 2015;91:72–83. [CrossRef]
[24] Raisinghania MD. Fluid dynamics with complete hydrodynamics and boundary layer theory. New Delhi: S. Chand Publishing; 2013.
[25] Ghadikolaei SS, Hosseinzadeh K, Hatami M, Ganji DD, Armin M. Investigation for squeezing flow of ethylene glycol ($C_2H_6O_2$) carbon nanotubes (CNTs) in rotating stretching channel with nonlinear thermal radiation. J Mol Liq 2018;263:10–21. [CrossRef]
[26] Chu YM, Nisar KS, Khan U, Daei Kasmaei H, Malaver M, Zaib A, et al. Mixed convection in MHD water-based molybdenum disulfide-graphene oxide hybrid nanofluid through an upright cylinder with shape factor. Water 2020;12:1723. [CrossRef]
[27] Lide DR, Kehiaian HV. CRC handbook of thermophysical and thermochemical data. Boca Raton: CRC Press; 2020. [CrossRef]
[28] Al-Sankoor K, Al-Gayyim H, Al-Musaedi S, Asadi Z, Ganji DD. Analytically investigating of heat transfer parameters with presence of graphene oxide nanoparticles in Williamson-magnetic fluid by AGM and HPM methods. Case Stud Therm Eng 2021;27:101236. [CrossRef]
[29] Elsaid K, Abdelkareem MA, Maghrabie HM, Sayed ET, Wilberforce T, Baroutaji A, et al. Thermophysical properties of graphene-based nanofluids. Int J Thermofluids 2021;10:100073. [CrossRef]
[30] Bejan A. Entropy generation minimization: The new thermodynamics of finite-size devices and finite-time processes. J Appl Phys 1996;79:1191–1218. [CrossRef]
[31] Bejan A, Kestin J. Entropy generation through heat and fluid flow. J Appl Mech 1983;50:475. [CrossRef]
[32] Paoletti S, Rispoli F, Sciubba E. Calculation of exergetic losses in compact heat exchanger passages. Proc ASME AES 1989;10:21–29.
[33] Bellman RE, Kalaba RE. Quasilinearization and nonlinear boundary value problems. New York: American Elsevier Publishing Company; 1965. [CrossRef]
[34] Canuto C, Hussaini MY, Quarteroni A, Zang TA. Spectral methods: Fundamentals in single domains. Berlin: Springer Berlin Heidelberg; 2006. [CrossRef]
[35] Malashetty MS, Umavathi JC, Prathap Kumar J. Convective magnetohydrodynamic two fluid flow and heat transfer in an inclined channel. Heat Mass Transf 2001;37:259–264. [CrossRef]
[36] Behseresht A, Noghrehabadi A, Ghalambaz M. Natural-convection heat and mass transfer from a vertical cone in porous media filled with nanofluids using the practical ranges of nanofluids thermo-physical properties. Chem Eng Res Des 2014;92:447–452. [CrossRef]
[37] Sinha KD, Chaudhary RC. Viscous incompressible flow between two coaxial rotating porous cylinders. Proc Nat Inst Sci India 1966;32:81.